

Maximum entropy mobility spectrum analysisfor the type-I Weyl semimetal TaAs

Wen-Chong Li(李文充), Ling-Xiao Zhao(赵凌霄), Hai-Jun Zhao(赵海军),Gen-Fu Chen(陈根富), and Zhi-Xiang Shi(施智祥)

Citation: Chin. Phys. B, 2022, 31 (**5**): 057103. DOI: 10.1088/1674-1056/ac2b24
Journal homepage: http://cpb.iphy.ac.cn; http://iopscience.iop.org/cpb

What follows is a list of articles you may be interested in

Intrinsic V vacancy and large magnetoresistance in $V_{1-\delta}Sb_2$ single crystal

Yong Zhang(张勇), Xinliang Huang(黄新亮), Jinglei Zhang(张警蕾), Wenshuai Gao(高文帅), Xiangde Zhu(朱相德), and Li Pi(皮雳)

Chin. Phys. B, 2022, 31 (**3**): 037102. DOI: 10.1088/1674-1056/ac3070

Heavy fermions in high magnetic fields

M Smidman, B Shen(沈斌), C Y Guo(郭春煜), L Jiao(焦琳), X Lu(路欣), H Q Yuan(袁辉球)

Chin. Phys. B, 2019, 28 (**1**): 017106. DOI: 10.1088/1674-1056/28/1/017106

Pressure effect in the Kondo semimetal $CeRu_4Sn_6$ with nontrivial topology

Jiahao Zhang(张佳浩), Shuai Zhang(张帅), Ziheng Chen(陈子珩), Meng Lv(吕孟), Hengcan Zhao(赵恒灿), Yi-feng Yang(杨义峰), Genfu Chen(陈根富), Peijie Sun(孙培杰)

Chin. Phys. B, 2018, 27 (**9**): 097103. DOI: 10.1088/1674-1056/27/9/097103

Electronic properties of defects in Weyl semimetal tantalum arsenide

Yan-Long Fu(付艳龙), Chang-Kai Li(李长楷), Zhao-Jun Zhang(张昭军), Hai-Bo Sang(桑海波), Wei Cheng(程伟), Feng-Shou Zhang(张丰收)

Chin. Phys. B, 2018, 27 (**9**): 097101. DOI: 10.1088/1674-1056/27/9/097101

Topological nodal line semimetals

Chen Fang(方辰), Hongming Weng(翁红明), Xi Dai(戴希), Zhong Fang(方忠)

Chin. Phys. B, 2016, 25 (**11**): 117106. DOI: 10.1088/1674-1056/25/11/117106

Maximum entropy mobility spectrum analysis for the type-I Weyl semimetal TaAs

Wen-Chong Li(李文充)[1], Ling-Xiao Zhao(赵凌霄)[2], Hai-Jun Zhao(赵海军)[1,†], Gen-Fu Chen(陈根富)[2], and Zhi-Xiang Shi(施智祥)[1,‡]

[1] *School of Physics and Key Laboratory of MEMS of the Ministry of Education, Southeast University, Nanjing* 211189, *China*
[2] *Beijing National Laboratory for Condensed Matter Physics, and Institute of Physics, Chinese Academy of Sciences, Beijing* 100190, *China*

(Received 18 July 2021; revised manuscript received 15 September 2021; accepted manuscript online 29 September 2021)

Due to non-saturating magnetoresistance (MR) and the special compensation mechanism, the Weyl semimetal TaAs single crystal has attracted considerable attention in condensed matter physics. Herein, we use maximum entropy mobility spectrum analysis (MEMSA) to extract charge carrier information by fitting the experimentally measured longitudinal and transverse electric transport curves of TaAs. The carrier types and the number of bands are obtained without any hypothesis. Study of the temperature dependence shows details of carrier property evolution. Our quantitative results explain the non-saturated magnetoresistance and Hall sign change phenomena of TaAs.

Keywords: Weyl semimetal, mobility spectrum analysis, magnetoresistance, electrical transportation

PACS: 71.55.Ak, 72.15.–v, 73.43.Qt **DOI:** 10.1088/1674-1056/ac2b24

1. Introduction

Studying new quantum materials such as topological insulators, Dirac materials and Weyl semimetals (WSMs) is of great importance in condensed matter physics because of their abundant physical properties and application potentials.[1–5] For WSMs, according to whether the Weyl cone is tilted, they can be divided into two categories: type-I and type-II. Recent first-principles calculations predicted a family of nonmagnetic WSM including TaAs, TaP, NbAs, and NbP.[6–11] Large magnetoresistance (MR) and low field Shubnikov–de Haas (SdH) oscillation were predicted.[8] These unique electronic structures and peculiar physical properties suggest that the WSM shows interesting physics and has potential future applications.

First-principles calculation predicted that TaAs is a type-I WSM with data-like W1 pockets and dot-like W2 pockets.[7] Ultrahigh mobility ($\mu_e \approx 18$ m$^2\cdot$V$^{-1}\cdot$s^{-1} at 10 K) and extremely large positive MR (80000% at 1.8 K in a field of 9 T) were discovered.[7] Surprisingly, negative MR is observed when the magnetic field is parallel to the current. Moreover, unlike ordinary metals or semiconductors, the SdH oscillations can be observed at a very low field. Detailed analysis indicates that there are two types of carrier in TaAs, in agreement with first-principles calculations.[6–8] However, how to quantitatively analyze the conducting behaviors of different types of fermions and how to study their evolution with temperature and magnetic field are still open questions, which may give answers to many interesting experimental observations including unsaturated MR and low field SdH oscillation.

Mobility spectrum analysis (MSA)[12–16] is a useful tool for extracting carrier information from experimentally measured longitudinal and transverse electric transport curves. It has previously been used for Ba(FeAs)$_2$ and FeSe superconductors[17,18] and type-II Weyl semimetals T$_d$-MoTe$_2$.[19] Recently, maximum entropy mobility spectrum analysis (MEMSA) has been used for β-PtBi$_2$.[20] Compared with other methods, MEMSA has higher resolution, and can perfectly fit the MR and Hall resistance data. In this paper, we use MEMSA to analyze the experimentally measured MR and Hall resistance of TaAs, from which mobility spectrum (MS) is obtained. MSA successfully distinguishes between the conductivity contributions of two different Weyl fermions (W1 and W2) at all experimentally measured temperatures. Our results give important clues for understanding the large and non-saturating MR in a TaAs single crystal.

2. Method

Within MS theory, the conductivity tensor is given by[14–18,20]

$$\sigma_{xx}(B) = \int_{-\infty}^{+\infty} \frac{s(\mu)}{1+(\mu B)^2}\,\mathrm{d}\mu, \tag{1}$$

$$\sigma_{xy}(B) = \int_{-\infty}^{+\infty} \frac{\mu B s(\mu)}{1+(\mu B)^2}\,\mathrm{d}\mu. \tag{2}$$

Here, $s(\mu) = e\mu\,\mathrm{d}n/\mathrm{d}u$ is the mobility spectrum, $n(\mu)$ is the density for carriers with mobility μ. Equations (1) and (2) can be solved numerically using MEMSA. Details of the method can be found in Refs. [15,20].

†Corresponding author. E-mail: haijunzhao@seu.edu.cn
‡Corresponding author. E-mail: zxshi@seu.edu.cn

© 2022 Chinese Physical Society and IOP Publishing Ltd

3. Results and discussion

3.1. Mobility spectrum of TaAs

The MS of TaAs for temperatures $T = 1.8$ K, 10 K, 40 K, 80 K, 100 K, and 120 K are shown in Figs. 1(a)–1(f), respectively. The corresponding fitting curves to experimentally measured magnetic conductivity $\sigma_{xx}(B)/\sigma_{xx}(0)$ and Hall conductivity $\sigma_{xy}(B)/\sigma_{xx}(0)$ are shown in Figs. 2(a) and 2(b). It is clear that MS nicely fits the experimental data, benefitting from the MEMSA method.

We now compare our MS results with reported first-principles calculations. According to Ref. [7], the band structure of TaAs contains a data-like Weyl pocket (W1) 21 meV below the Fermi surface, and a dot-like Weyl pocket (W2) about 2 meV above the Fermi surface. Therefore, the dominant carrier is the electron for W1, and is the hole for W2. At low temperatures ($T < 40$ K), our MS also contains two dominant pockets: one electron pocket and one hole pocket (see Figs. 1(a)–1(c)). Therefore, we mark the big electron peak with e_{W1}, and the big hole peak with h_{W2}. Holes for W1 and electrons for W2, in principle, can be thermally activated. There are two small peaks on our MS at low temperature T, which grow big after increasing T. Therefore, they very likely originate from W1 and W2 (we mark them with h_{W1} and e_{W2}, respectively). Other carriers coming from ordinary pockets should have mobilities that are smaller than that of the best normal metal conductors (e.g., $\mu \approx 0.6$ m^2·V^{-1}·s^{-1} for silver at 5 K[21]). No such peak with small mobilities is observed in our MS curves, indicating that conductivity contributions from ordinary pockets are too small to be detected by transport measurement.

The MS is sensitive to temperature. In general, with increasing temperature T, the number of peaks remains unchanged for $T > 120$ K (see Figs. 1(a)–1(f)). However, peak positions (corresponding to mobilities) as well as heights (corresponding to charge densities), greatly vary with temperature. For peak positions, as shown in Figs. 1(a)–1(f), almost all peaks move toward the low mobility direction (i.e., mobilities decrease) as temperature increases. However, the mobility of e_{W1} decreases faster than that of h_{W2}.

As a result, gradually, the mobility of h_{W2} approaches that of e_{W1}, and the MS becomes symmetric. For peak heights, the peaks of e_{W1} and h_{W2} decrease with increasing temperature, whereas those of e_{W2} and h_{W1} increase. At high temperatures ($T > 40$ K), the height of all four peaks is equal.

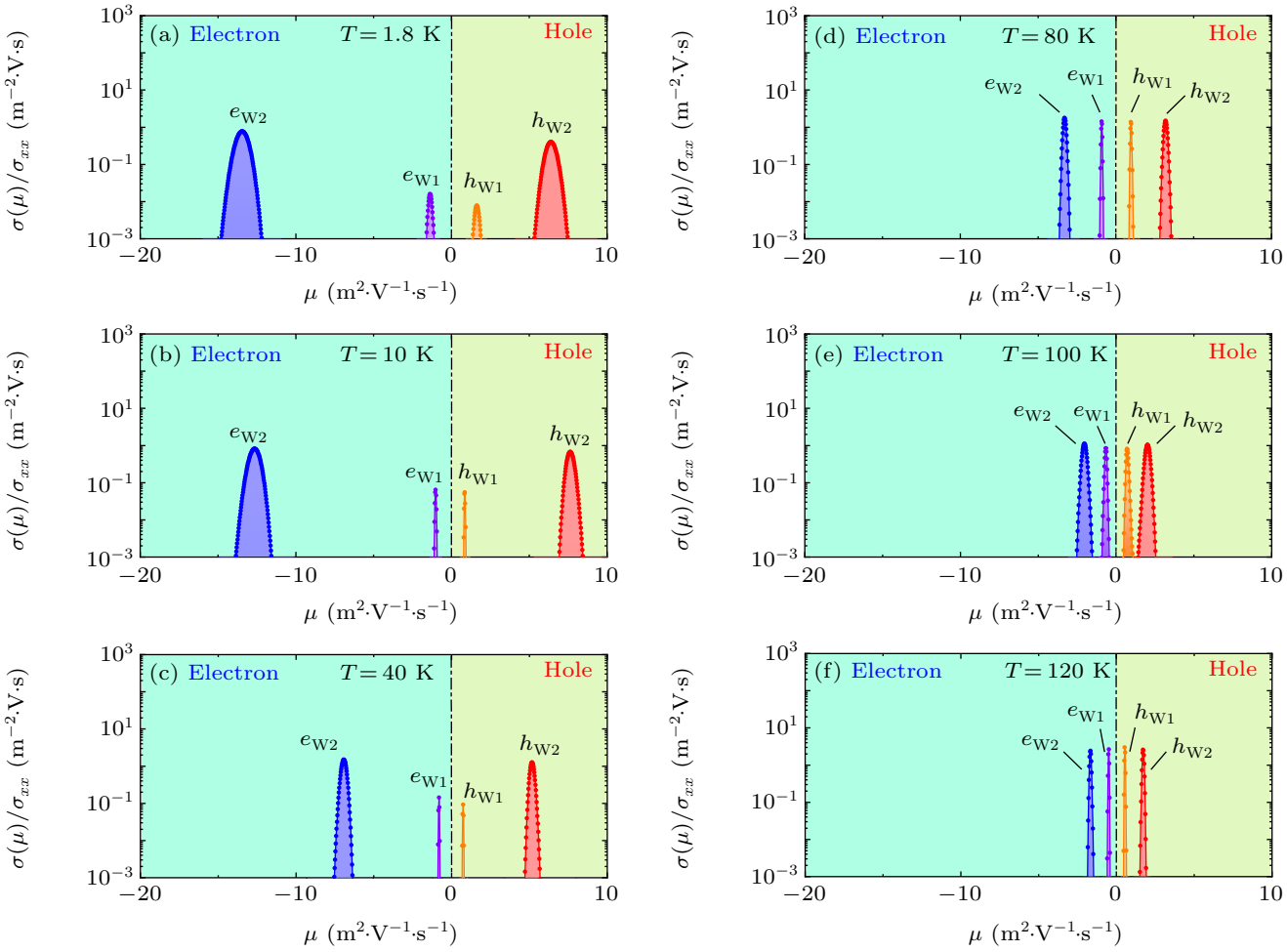


Fig. 1. The MS of TaAs displayed in semi-logarithmic scale for temperature of (a) 1.8 K, (b) 10 K, (c) 40 K, (d) 80 K, (e) 100 K, and (f) 120 K.

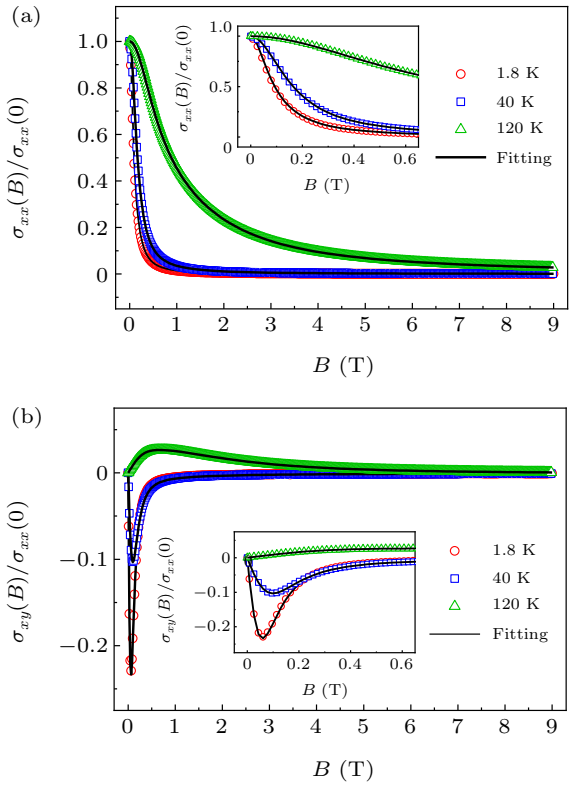


Fig. 2. Normalized experimental magnetic conductivity (a) $\sigma_{xx}(B)/\sigma_{xx}(0)$ and (b) Hall conductivity $\sigma_{xy}(B)/\sigma_{xx}(0)$ at 1.8 K, 10 K, 40 K, 80 K, 100 K, and 120 K (dots), and its MEMSA fitting (solid lines).

3.2. Temperature dependence of mobility, carrier density, and conductivity contributions

To further explore the temperature dependence of MS, we calculate the mobilities, carrier densities, and conductivity contributions from MS and present them in Figs. 3(a)–3(c).

The mobilities for each type of carriers are calculated by taking the peak values. At the lowest temperature $T = 1.8$ K, for W1 fermions, $e_{\rm W1}$ has a very high mobility ($\mu^{\rm e}_{\rm W1} = 13.44$ m$^2\cdot$V$^{-1}\cdot$s^{-1}), which is close to the mobilities of Dirac fermions in Dirac materials such as graphene ($\mu = 20$ m$^2\cdot$V$^{-1}\cdot$s^{-1}), and is slightly smaller than the value estimated by SdH oscillation ($\mu = 18$ m$^2\cdot$V$^{-1}\cdot$s^{-1}).[7] The mobility of $h_{\rm W1}$ is lower ($\mu^{\rm h}_{\rm W1} = 1.64$ m$^2\cdot$V$^{-1}\cdot$s^{-1}), but it is still much larger than the mobility of carriers in silver, and is close to Dirac-like fermions in $PtBi_2$.[20] For W2 fermions, the mobility of $h_{\rm W2}$ $\mu^{\rm h}_{\rm W2} = 6.39$ m$^2\cdot$V$^{-1}\cdot$s^{-1}, which is about half of $\mu^{\rm e}_{\rm W1}$, whereas that of $e_{\rm W2}$, $\mu^{\rm e}_{\rm W2} = 1.36$ m$^2\cdot$V$^{-1}\cdot$s^{-1}, which is comparable to $\mu^{\rm h}_{\rm W1}$. When changing the temperature, as shown in Fig. 3(a), low mobility fermions, i.e., $\mu^{\rm e}_{\rm W2}$ and $\mu^{\rm h}_{\rm W1}$, are almost temperature independent. For high mobility fermions, i.e., $\mu^{\rm e}_{\rm W1}$ and $\mu^{\rm h}_{\rm W2}$, on the contrary, in general, the mobility decreases significantly with increasing temperature, except that $\mu^{\rm h}_{\rm W2}$ increases slightly at $T = 10$ K. The decrease of mobilities for W2 is probably due to increased thermal scattering. $\mu^{\rm e}_{\rm W1}$ decreases faster than $\mu^{\rm h}_{\rm W2}$ for $T < 80$ K, but $\mu^{\rm e}_{\rm W1} \approx \mu^{\rm h}_{\rm W2}$ for $T > 80$ K, which is consistent with the symmetric MS shown in Figs. 1(d)–1(f).

In Fig. 3(b), we show carrier densities as a function of temperature. Carrier densities for mobility $\mu \in [a,b]$ can be calculated by

$$n = \int_a^b s(\mu)/(e\mu)\,{\rm d}\mu.$$

By taking a and b to be the lower and upper boundary of a specific peak, this integral gives its carrier density. For $T < 40$ K, the carrier densities of big peaks, i.e., $n^{\rm e}_{\rm W1}$ for $e_{\rm W1}$ and $n^{\rm h}_{\rm W2}$ for $h_{\rm W2}$, are almost independent of temperature, and their values are 2 orders less than many other reported large magnetoresistance topological materials, such as pyrite $PtBi_2$,[20] WTe_2[22] and LaSb,[23] but are similar to Cr_3As_2.[24] The charge densities for the two small peaks ($n^{\rm e}_{\rm W2}$ for $e_{\rm W2}$ and $n^{\rm h}_{\rm W1}$ for $h_{\rm W1}$) are 1 order smaller.

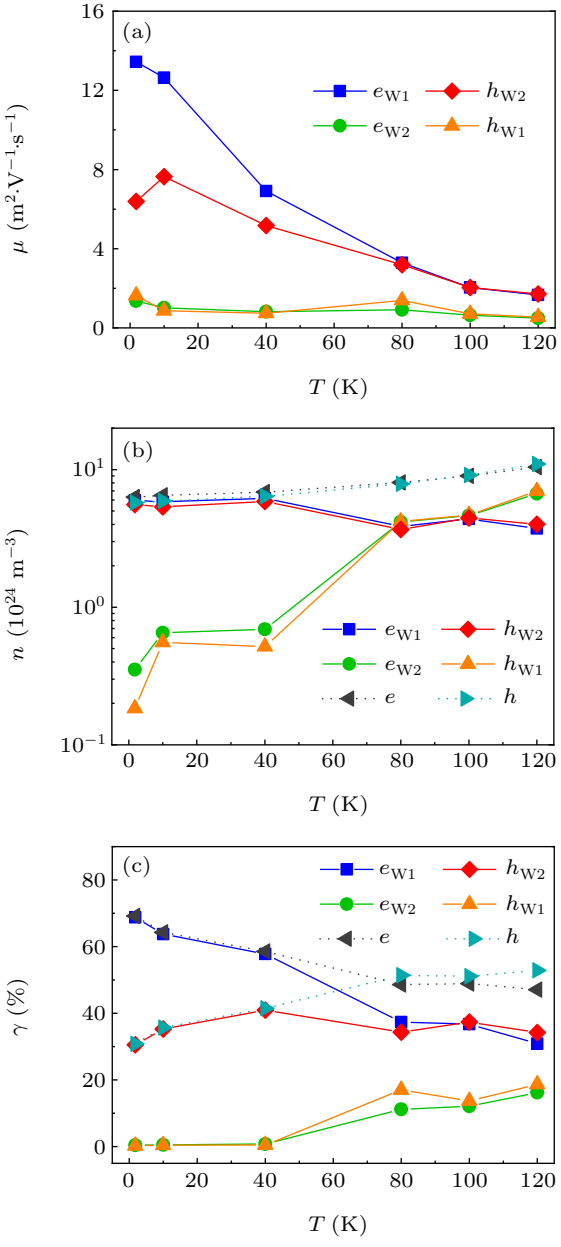


Fig. 3. (a) The temperature dependence of mobilities μ, (b) carrier densities n, (c) RCC at zero field γ.

For higher temperatures, the charge densities for the two big peaks n^{e}_{W1} and n^{h}_{W2} decrease with increasing temperature, whereas that of small peaks (n^{e}_{W2} and n^{h}_{W1}), as well as total density of electrons and holes ($n^{h}_{W} = n^{h}_{W1} + n^{h}_{W2}$ and $n^{e}_{W} = n^{e}_{W1} + n^{e}_{W2}$), increase (see Fig. 3(b)).

The conductivity contribution for carrier with $\mu \in [a,b]$ at zero field is given by

$$\sigma(a,b) = \int_{a}^{b} s(\mu)\,\mathrm{d}\mu.$$

Then, the ratio of the conductivity contribution (RCC) $\gamma(a,b)$ can be calculated by $\gamma(a,b) = \sigma(a,b)/\sigma(-\infty,+\infty)$. Similar to charge densities, by choosing suitable values of a and b, the ratio of conductivity contribution γ for each peak is achieved. As shown in Fig. 3(c), at low temperatures, the RCC for the two big peaks, γ^{e}_{W1} and γ^{n}_{W2} are large, whereas the RCC for the two thermally activated small peaks, γ^{e}_{W2} and γ^{n}_{W1}, are almost zero. When the temperature increases, γ^{e}_{W1} decreases while γ^{n}_{W2} almost remains unchanged. γ^{e}_{W2} and γ^{n}_{W1} start to increase for $T > 40$ K. The total RCC for electrons γ^{e}_{W} decreases as the temperature increases, whereas that for holes γ^{e}_{W} increases. Information of every peak for various temperatures is summarized in Table 1.

Table 1. Summery of carrier information: contribution to the conductivity γ, average mobility μ, and change concentration n.

T		Electrons		Holes	
		e_{W1}	e_{W2}	h_{W1}	h_{W2}
1.8 K	γ	68.8%	0.4%	0.3%	30.5%
	μ ($m^2 \cdot V^{-1} \cdot s^{-1}$)	13.444	1.363	1.638	6.391
	n (m^{-3})	6.0×10^{24}	3.5×10^{23}	1.8×10^{23}	5.6×10^{24}
10 K	γ	63.7%	0.6%	0.4%	35.3%
	μ ($m^2 \cdot V^{-1} \cdot s^{-1}$)	12.644	1.013	0.863	7.641
	n (m^{-3})	5.8×10^{24}	6.5×10^{23}	5.6×10^{23}	5.4×10^{24}
40 K	γ	57.7%	0.8%	0.5%	41.2%
	μ ($m^2 \cdot V^{-1} \cdot s^{-1}$)	6.916	0.813	0.738	5.165
	n (m^{-3})	6.2×10^{24}	6.9×10^{23}	5.2×10^{23}	5.9×10^{24}
80 K	γ	39.3%	11.8%	12.7%	36.2%
	μ ($m^2 \cdot V^{-1} \cdot s^{-1}$)	3.289	0.913	1.384	3.189
	n (m^{-3})	3.9×10^{24}	4.2×10^{24}	4.2×10^{24}	3.7×10^{24}
100 K	γ	36.5%	12.5%	13.8%	37.2%
	μ ($m^2 \cdot V^{-1} \cdot s^{-1}$)	2.039	0.638	0.713	2.039
	n (m^{-3})	4.4×10^{24}	4.6×10^{24}	4.7×10^{24}	4.5×10^{24}
120 K	γ	30.9%	16.2%	18.7%	34.2%
	μ ($m^2 \cdot V^{-1} \cdot s^{-1}$)	1.663	0.488	0.538	1.713
	n (m^{-3})	3.7×10^{24}	6.7×10^{24}	7.0×10^{24}	4.0×10^{24}

3.3. Field dependence of the conductivity contribution

To analyze the ultra-high MR of TaAs, we calculate the field dependence of σ_{xx} for each peak by substituting $s(\mu)$ of each peak back to Eq. (1). For $\mu B \gg 1$, $\sigma_{xx} \propto (\mu B)^{-2} \approx 0$. Therefore, the initially dominated high mobility carriers will be localized after increasing field, while the localization of the low mobility carriers is weak. As a result, low mobility carriers become dominant. This behavior leads to a crossover of the conductivity contribution as a function of field for different bands. If an initially hole-dominated conductivity becomes electron-dominated at a high field (vice versa), the Hall conductivity sign changes. For complex MS, the sign change can even appear more than once. If ultra-high mobility carriers dominate the conductivity (e.g., our TaAs sample at low temperature), even a very low field is capable of localizing the conducting carriers, thus, greatly decreasing conductivity, causing a field-induced conductor to insulator transition (CIT),[25–28] and generating extremely large MR.

For TaAs, the conductivities of each type of carriers as a function of field are shown in Fig. 4. At $T = 1.8$ K, the ultra-high mobility of e_{W1} causes a very fast localization. As shown in Fig. 4(a), the crossover of the conductivity contribution of e_{W1}, and h_{W2} appears at a field as low as $B = 0.12$ T (see the intersection of σ_{xx} for e_{W2} and h_{W2}). This illustrates that the dominant carrier is the electron-like W1 fermion when $B > 0.12$ T, but it is the hole-like W2 fermion when $B > 0.12$ T. Therefore, the Hall conductivity sign changes. For a high field limit, $\sigma_{xx}(B) \approx [\sigma_{xx}(0)\mu^{-2}]B^{-2} = KB^{-2}$, where K is a parameter that determines dominant carriers at high field. Therefore, due to the extremely low $\sigma_{xx}(0)$ of thermal-activated fermions, their K value is always smaller than that of the preexisting fermions e_{W1} and h_{W2}. Therefore, the thermal-activated fermions always have a lower contribution to the conductor for various fields.

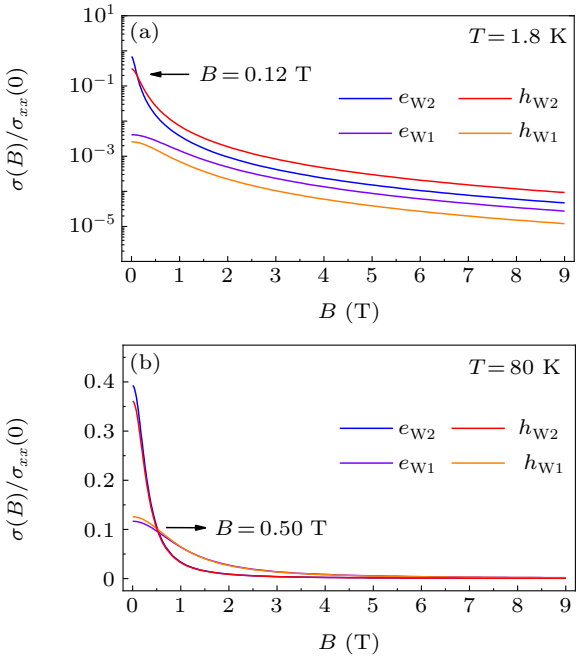


Fig. 4. (a) The conductivity contributions vary with the magnetic field for $T = 1.8$ K (a), and $T = 80$ K (b), respectively.

At 80 K, as was discussed previously, the mobility and density of the electron equals that of the hole for both W1 and W2. Therefore, the $\sigma_{xx}(B)$ of the electron always overlaps with the hole (see Fig. 4(b)), so we cannot easily identify

the dominant carrier between the electron-like and hole-like carriers. However, compared with the low temperature case, the conductivity for thermal-activated fermions is greatly enhanced. Due to their low mobilities, their K values become larger than those of preexisting fermions. Therefore, an intersection of $\sigma_{xx}(B)$ for thermal-activated fermions and preexisting fermions appears (at $B = 0.5$ T), indicating that the preexisting fermion-dominated conductivity becomes thermal-activated-fermion dominant when $B > 0.5$ T.

4. Conclusion

In summary, we use MEMSA to study the carrier properties of the type-I Weyl semimetal TaAs by fitting the experimentally measured longitudinal and transverse electric transport curves. At low temperature, we discovered four peaks: two big peaks and two small peaks (each containing one electron peak and one hole peak). Upon increasing the temperature, the two small peaks grow, showing that they are thermal-activated fermions. By comparing with reported first-principles results, the following peaks are identified: big electron peak and the small hole peak correspond to Weyl-I and the other two correspond to Weyl-II. Further quantitative calculation of mobility, carrier density, and RCC for varying temperatures shows that at low temperatures, the two dominant peaks have very high mobilities, which decrease with increasing temperature, whereas the carrier densities are insensitive to temperature change until $T > 40$ K. However, the carrier densities of the two small peaks quickly increase with temperature, indicating that they are thermal-activated fermions. The increased carrier density also increases their RCC. Our results explain the Hall sign change phenomenon, and shows the origin of non-saturating magnetoresistance.

Acknowledgment

Project supported by the National Natural Science Foundation of China (Grant Nos. 11674054, U1932217, and 11704067).

References

[1] Yan B and Felser C 2017 *Annu. Rev. Condens. Matter Phys.* **8** 337
[2] Wang Z H, Yang L, Li X J, Zhao X T, Wang H L, Zhang Z D and Gao X P A 2014 *Nano Lett.* **14** 6510
[3] Yang B J and Nagaosa N 2014 *Nat. Commun.* **5** 4898
[4] Young S M, Zaheer S, Teo J C Y, Kane C L, Mele E J and Rappe A M 2012 *Phys. Rev. Lett.* **108** 140405
[5] Tang P, Zhou Q, Xu G and Zhang S C 2016 *Nat. Phys.* **12** 1100
[6] Weng H, Fang C, Fang Z, Bernevig B A and Dai X 2015 *Phys. Rev. X* **5** 011029
[7] Huang X, Zhao L, Long Y, Wang P, Chen D, Yang Z, Liang H, Xue M, Weng H, Fang Z, Dai X and Chen G 2015 *Phys. Rev. X* **5** 031023
[8] Lee C C, Xu S Y, Huang S M, Sanchez D S, Belopolski I, Chang G, Bian G, Alidoust N, Zheng H, Neupane M, Wang B, Bansil A, Hasan M Z and Lin H 2015 *Phys. Rev. B* **92** 235104
[9] Lv B Q, Muff S, Qian T, Song Z D, Nie S M, Xu N, Richard P, Matt C E, Plumb N C, Zhao L X, Chen G F, Fang Z, Dai X, Dil J H, Mesot J, Shi M, Weng H M and Ding H 2015 *Phys. Rev. Lett.* **115** 217601
[10] Lv B Q, Xu N, Weng H M, Ma J Z, Richard P, Huang X C, Zhao L X, Chen G F, Matt C E, Bisti F, Strocov V N, Mesot J, Fang Z, Dai X, Qian T, Shi M and Ding H 2015 *Nat. Phys.* **11** 724
[11] Du J, Wang H, Chen Q, Mao Q, Khan R, Xu B, Zhou Y, Zhang Y, Yang J, Chen B, Feng C and Fang M 2016 *Sci. China Phys. Mech. Astron.* **59** 657406
[12] McClure J W 1956 *Phys. Rev.* **101** 1642
[13] McClure J W 1958 *Phys. Rev.* **112** 715
[14] Beck W A and Anderson J R 1987 *J. Appl. Phys.* **62** 541
[15] Rothman J, Meilhan J, Perrais G, Belle J P and Gravrand O 2006 *J. Electron. Mater.* **35** 1174
[16] Kiatgamolchai S, Myronov M, Mironov O A, Kantser V G, Parker E H C and Whall T E 2002 *Phys. Rev. E* **66** 036705
[17] Huynh K K, Tanabe Y, Urata T, Heguri S, Tanigaki K, Kida T and Hagiwara M 2014 *New J. Phys.* **16** 093062
[18] Huynh K K, Tanabe Y, Urata T, Oguro H, Heguri S, Watanabe K and Tanigaki K 2014 *Phys. Rev. B* **90** 144516
[19] Pei Q L, Luo X, Chen F C, Lv H Y, Sun Y, Lu W J, Tong P, Sheng Z G, Han Y Y, Song W H, Zhu X B and Sun Y P 2018 *Appl. Phys. Lett.* **112** 072401
[20] Zhao H, Li W, Chen Y, Xu C, Li B, Luo W, Qian D and Shi Z 2021 *Sci. Rep.* **11** 6249
[21] Kobayashi K and Brown F C 1959 *Phys. Rev.* **113** 507
[22] Ali M N, Xiong J, Flynn S, Tao J, Gibson Q D, Schoop L M, Liang T, Haldolaarachchige N, Hirschberger M, Ong N P and Cava R J 2014 *Nature* **514** 205
[23] Tafti F F, Gibson Q D, Kushwaha S K, Haldolaarachchige N and Cava R J 2016 *Nat. Phys.* **12** 272
[24] Liang T, Gibson Q, Ali M N, Liu M, Cava R J and Ong N P 2015 *Nat. Mater.* **14** 280
[25] Bolotin K I, Sikes K J, Jiang Z, Klima M, Fudenberg G, Hone J, Kim P and Stormer H L 2008 *Solid State Commun.* **146** 351
[26] Blomqvist H and Noréus D 2002 *J. Appl. Phys.* **91** 5141
[27] Obrzut J, Douglas J F, Kharchenko S B and Migler K B 2007 *Phys. Rev. B* **76** 195420
[28] Ahadi K, Nemati A and Mahdavi S M 2012 *Mater. Lett.* **83** 124